

PROCEEDINGS OF SPIE

[SPIDigitalLibrary.org/conference-proceedings-of-spie](https://spiedigitallibrary.org/conference-proceedings-of-spie)

Plasma halogenated a-C:H as growth inhibiting layer for ASD of titanium oxide

Krishtab, M., Hung, J., Koret, R., Turovets, I., Shah, K., et al.

M. Krishtab, J. Hung, R. Koret, I. Turovets, K. Shah, S. Rangarajan, L. Warad, V. Zhang, R. Ameloot, S. Armini, "Plasma halogenated a-C:H as growth inhibiting layer for ASD of titanium oxide," Proc. SPIE 11325, Metrology, Inspection, and Process Control for Microlithography XXXIV, 113250Y (15 May 2020); doi: 10.1117/12.2551492

SPIE.

Event: SPIE Advanced Lithography, 2020, San Jose, California, United States

Plasma Halogenated a-C:H as Growth Inhibiting Layer for ASD of Titanium Oxide

M. Krishtab^{a,b}, J. Hung^c, R. Koret^d, I. Turovets^d, K. Shah^c, S. Rangarajan^c, L. Warad^c, V. Zhang^c, R. Ameloot^b and S. Armini^a

^a IMEC, Kapeldreef 75, 3001 Heverlee, Belgium; ^b Centre for Surface Chemistry and Catalysis, KU Leuven, Celestijnenlaan 200F, 3001 Leuven, Belgium; ^c Nova Measuring Instruments, Inc., 3090 Oakmead Village Dr., Santa Clara, CA 95051, USA; ^d Nova Measuring Instruments, LTD, P.O. Box 266, Weizmann Science Park, Rehovot 76100, Israel

ABSTRACT

The native self-alignment of area-selective deposition (ASD) processes makes this technology a promising solution for precise pattern positioning in the EUV era. The key challenge for any ASD process is its defectivity associated with the deposition on the growth-inhibiting surface. Therefore, the ability to qualify an ASD process using the appropriate set of in-line metrology tools is crucial for up-scaling of the technology. In this work, we present a new concept of area-selective ALD TiO₂ growth and use it as an example to show the potential of in-line OCD and XPS tools for evaluation of ASD processes. The proposed novel process is based on selective growth of TiO₂ on top of SiO₂/SiN in the presence of plasma halogenated amorphous carbon (a-C:H) acting as a growth-inhibiting layer. The exposure of a-C:H to CF₄ or Cl₂ plasma results in formation of a thin halogen-rich film suppressing nucleation of TiO₂, while the latter is minimally affected on the plasma treated SiN_x or SiO₂ layers. The selectivity was assessed on both blanket films and 45 nm half-pitch a-C:H line patterns. The analysis of blanket a-C:H substrates showed that the plasma chlorination provides a substantially more efficient growth inhibition as compared to the fluorination. However, the ability of the CF₄-plasma to etch the topmost surface of the a-C:H makes it more favorable for application on a-C:H patterns, surface of which is typically contaminated with residues from hard-mask or from the patterning plasma. Therefore, the pre-cleaning of the a-C:H line pattern surface with CF₄-plasma is required to restore the growth blocking efficiency of the chlorinated a-C:H.

Keywords: area-selective deposition, ALD, amorphous carbon, defectivity, OCD, XPS, in-line metrology

1. INTRODUCTION

Over the last few years, the area-selective deposition technology received a lot of attention from the microelectronics research community as a potential solution for pattern misalignment issues. The growth of the functional layers in predefined areas can ease the edge placement error requirements^{1,2}, allow a simple tone inversion scheme³, enable a reliable metal passivation⁴ etc. One of the most common ways to achieve the selective deposition is to employ the combination of surface-sensitive atomic-layer deposition (ALD) method with growth inhibitors such as organic self-assembly monolayers (SAMs)⁵. Despite their versatility and inherent selectivity to dielectric or metal surfaces, the formation of a perfect monolayer over a large area is often challenged by the complex assembly dynamics and by the monolayer's domain structure⁶. In this study, we propose to employ the surface of amorphous carbon (a-C:H) modified by a low power halogen-based plasma as an analog of inhibiting SAMs layers. One of the key advantages of this approach is its affordability since it involves materials and tools which are commonly available in every microelectronics fab. Moreover, the combination of etching and ALD chambers in a single platform would enable intermediate a-C:H surface regeneration within ALD supercycles^{7,8}, which could significantly enhance the process selectivity. We demonstrated the viability of the halogenated a-C:H as an inhibition layer for nucleation of ALD TiO₂ in the context of the tone inversion scheme shown in Figure 1.

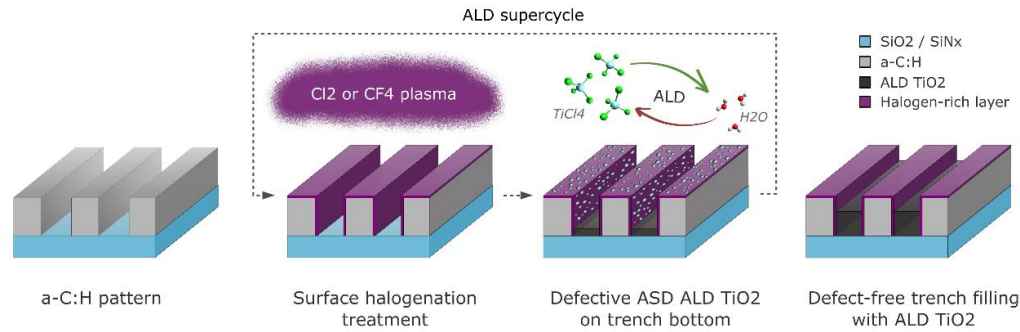


Figure 1. The proposed approach for area-selective deposition of ALD TiO₂ featuring plasma halogenated amorphous carbon as a non-growth surface and an ALD supercycle scheme based on intermediate halogenation plasma treatment.

Besides the validation of the proposed approach, another related goal of the work was to assess the possibility of the ASD process control using in-line metrology techniques such as top-down SEM, OCD and XPS. The key characteristic of any ASD process is its selectivity S , which is defined as follows:

$$S = \frac{\Theta_{GA} - \Theta_{NGA}}{\Theta_{GA} + \Theta_{NGA}} \quad (1)$$

where Θ_{GA} and Θ_{NGA} are the amounts of material deposited in the desired growth area and non-growth area, respectively⁹. Therefore, the ability to measure the amount of the deposited material on both types of surfaces is essential for metrology used to qualify the process. While rather trivial on blanket surfaces, this task becomes challenging when the growth and non-growth areas are put next to each other in the form of a regular pattern with pitches of few tens of nanometers or below. The analysis of an ASD process on patterns conventionally involves X-SEM or TEM. Also the self-focusing SIMS technique achieving resolution down to 20 nm was recently proposed¹⁰. However, none of the above techniques may provide non-destructive in-line analysis of the process selectivity which would be essential for upscaling of the ASD technology and for increasing of its research throughput.

2. MATERIALS AND METHODS

2.1 Amorphous carbon

The a-C:H films under study were deposited on Applied Materials Producer® platform. The a-C:H films of 100 nm were used for experiments on blanket films. The 90 nm pitch line pattern of a-C:H was prepared from a stack composed of Si-substrate/ 50 nm PECVD SiN_x/ 80 nm a-C:H/ 15 nm PEALD SiO₂ hard-mask. The latter was removed by wet cleaning in 0.5% aqueous HF solution following the a-C:H patterning with He/H₂ plasma.

2.2 Plasma halogenation

The plasma halogenation process was performed on TEL TACTRAS® platform using a low-power CCP plasma. The duration of CF₄ and Cl₂ plasmas was optimized to have minimal loss of a-C:H during the surface halogenation (< 2 nm). The chlorination process was preceded by an additional short H₂-plasma activation treatment.

2.3 Area-selective deposition of ALD TiO₂

The ALD TiO₂ process based on sequential pulsing of TiCl₄ and H₂O precursors was realized at 200°C (susceptor temperature) in EmerALD® chamber from ASM International. The estimated growth rate on SiO₂ substrate was 0.035 nm/cycle. The ALD supercycles considered in the current study included regeneration plasma treatment which was the same as the initial plasma halogenation unless stated otherwise.

2.4 ASD process characterization

Rutherford backscattering spectroscopy (RBS) was used to estimate the thickness of TiO₂ deposited on blanket substrates. The spectra of He⁺ ions accelerated to 1.523 MeV and backscattered at an angle 170° was recorded with a silicon surface

barrier (SSB) detector in a customized scattering chamber developed at the Jülich Research Center. In-house developed analysis software was used to fit the spectra and to deduce the areal density of Ti. The TiO₂ thickness was then estimated by assuming anatase phase of the growing TiO₂ layer.

Atomic force microscopy (AFM) topography images (1 x 1 μm², 256 x 256 pixels) were recorded in tapping mode with Dimension Edge microscope (Bruker). The image corrections (rows alignment, horizontal scars elimination) and plotting was performed with Gwyddion 2.44 software¹¹. The defect maps highlighting the nucleation of ALD TiO₂ on non-growth halogenated a-C:H surface were obtained by marking the pixels exceeding the threshold value equal to 5σ, where σ is the root mean square roughness of the halogenated a-C:H surface before deposition of TiO₂. The selected threshold criterion presents the lower bound estimate of the TiO₂ nucleation defects.

The top-down SEM images were collected on a Hitachi GC4000 system.

Scatterometry also known as Optical CD (OCD) was used to measure the TiO₂ thickness deposited on the SiN_x surface inside the a-C:H array. The T600MMSR, by Nova Measuring Instruments, was the selected OCD platform in this work. The system illuminates a broadband wavelength from UV to IR and is supporting a multiple polarization and azimuthal angles measurements. Rigorous coupled-wave analysis (RCWA) was used to solve the scattering from the a-C:H array and to extract the TiO₂ thickness.

The VeraflexTM in-line XPS + XRF system was used to characterize the changes in the composition of surfaces exposed to halogenation plasma as well as to quantify the amount of TiO₂ on both growth and non-growth surfaces. The XPS spectra were directly collected on patterned line-space features. A combination of elemental analysis and proprietary algorithms was used to complete the analysis.

3. RESULTS AND DISCUSSION

3.1 ASD on blanket layers

The initial validation of the proposed tone inversion concept was done on blanket films of native SiO₂ and halogenated a-C:H. The presence of TiO₂ on the surfaces was detected using RBS (Figure 2a). While the growth of TiO₂ on the SiO₂ surface proceeded linearly as a function of the ALD cycles number, there was a pronounced delay in nucleation of TiO₂ on top of fluorinated and chlorinated a-C:H. The latter exhibited nearly no presence of TiO₂ on the surface even after 450 cycles. The noticeable nucleation of TiO₂ on the fluorinated a-C:H started after 150 cycles. On the other hand, the growth inhibition on the fluorinated a-C:H was significantly improved when 300 cycles were split in 5 supercycles, deposition rounds each followed by the corresponding halogenation plasma treatment.

The addition of the intermediate plasma treatment also had an impact on the TiO₂ deposited on top of SiO₂. The reduced growth rate indicates the etching of TiO₂ during the fluorination plasma treatment. The slowing down of the TiO₂ growth is less apparent in the case of the cyclic chlorination process. The effect of the supercycle approach is particularly evident in Figure 2a. It provides a comparison of the TiO₂ nucleation defect maps on the non-growth surfaces between the 300 cycles ALD processes realized in a single step or in 5 supercycles. The capability of the fluorination process to etch the TiO₂ nucleation defects results in strongly reduced process defectivity, while the blocking performance of the chlorination process shows no apparent improvement when intermediate halogenation treatments were introduced.

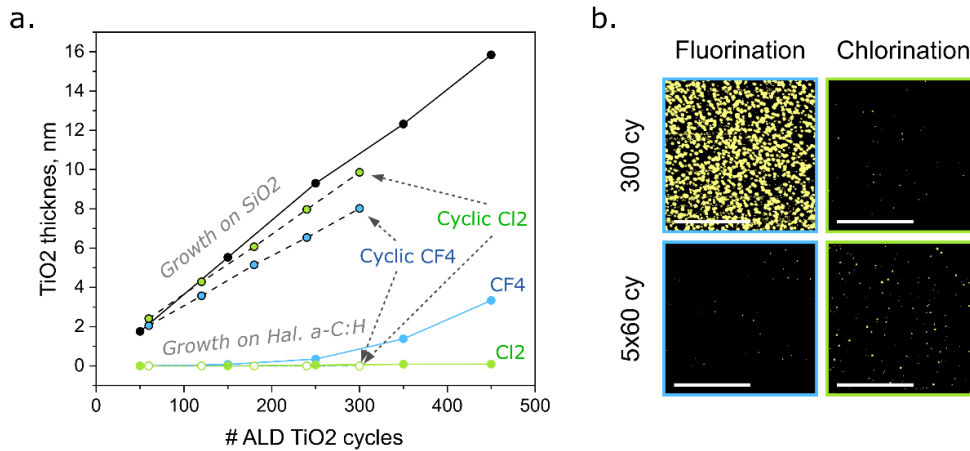


Figure 2. Selectivity and defectivity of the proposed ASD ALD TiO₂ process tested on blanket films: (a) thickness of ALD TiO₂ measured on SiO₂ and on halogenated amorphous carbon surfaces with RBS; (b) defect map obtained from AFM topography images by threshold marking (5 σ), the scalebar on the images is 500 nm.

3.2 ASD on patterns

The next level of the concept validation is the assessment of the process selectivity on patterns of halogenated a-C:H. It is important to note that the surface composition of the patterned a-C:H may deviate from that of the blanket a-C:H film as a result of the fabrication process involving a hard-mask deposition and a direct interaction with an etching plasma. Therefore, the validity of the concept could not be simply assumed based on the promising results discussed in the previous section.

We studied the deposition of ALD TiO₂ on top of the halogenated a-C:H line pattern landing on SiN_x layer using both single step deposition (100 cycles, 200 cycles and 300 cycles) and the supercycle approach (3 rounds of 100 cycles). The duration of the fluorination treatment embedded in the supercycles was three times shorter as compared to the standard a-C:H fluorination process. This change in the experiment was supposed to minimize the potential impact of the CF₄ plasma on the a-C:H trench width.

The inspection of the top surface with SEM is the simplest and the fastest way to get the first impression of the process selectivity. The top-down SEM images do not allow a straightforward analysis of the TiO₂ nucleation on the sidewalls of the a-C:H pattern and provide no information regarding the TiO₂ growth at the bottom of the trenches. Nonetheless, they give some insightful clues about the selectivity trends which can be further explored using more sophisticated metrology techniques. For example, the SEM images shown in Figure 3 suggest a better growth blocking efficiency of the fluorination treatment as compared to the chlorination, in contrast with the earlier observations on the a-C:H blanket films. Also, one can notice a rather limited value of the supercycle approach in this experiment. The lack of its efficiency previously demonstrated on blanket films could be explained by the increased length of the supercycle along with the shortened fluorination plasma treatment.

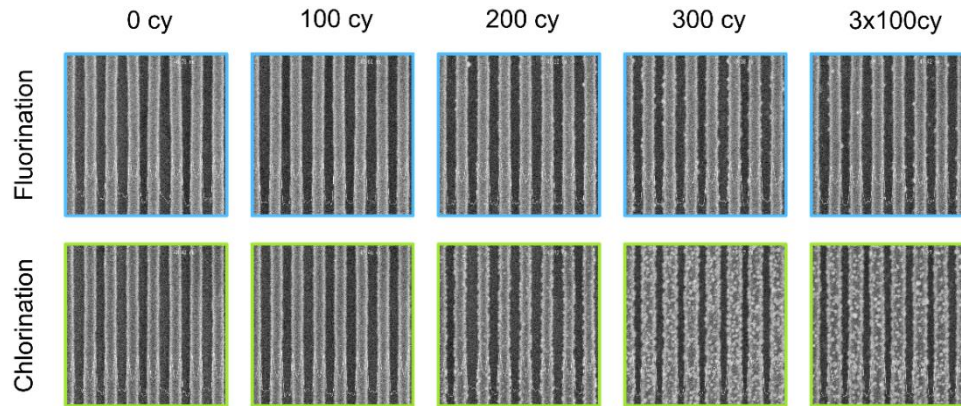


Figure 3. Top-down SEM images of 90 nm pitch a-C:H line pattern after plasma halogenation and deposition of ALD TiO₂ within a single process (100 cycles, 200 cycles, 300 cycles) or via three ALD supercycles (3x100 cycles).

The analysis of the same line pattern using OCD models allows to capture the deposition of ALD TiO₂ at the bottom of the trenches, i. e. on top of SiN_x surface representing the growth area (Figure 4a). The obtained OCD results are compared with the expected values of TiO₂ thickness measured with spectroscopic ellipsometry (SE) on the same wafers at pattern-free areas exposing SiN_x. In the case of the chlorination treatment, the OCD data match very well the results of the thin film measurements. Although similar trends in evolution of the TiO₂ thickness are demonstrated by both OCD and SE on fluorinated wafers, the OCD thickness values in arrays tend to be 2-4 nm larger than the thickness of TiO₂ measured on thin films. Taking into account the previously mentioned etching capability of the fluorination plasma, one can assume the presence of a more complex SiN_x profile at the trench bottom of the fluorinated a-C pattern. This change in the profile can allow selective deposition not only on SiN_x in the bottom of a-C pattern, but also on the walls of the SiN_x trench created by the CF₄ plasma. This additional growth may be responsible for the difference between the OCD thickness values measured in arrays and the thickness of TiO₂ measured at blanket targets, thus showing the importance of process control at array targets by OCD. As a high-throughput in-line analysis technique, OCD is also capable of providing full wafer maps of TiO₂ thickness formed within the trenches. The collected maps for chlorinated and fluorinated a-C:H demonstrate similar TiO₂ thickness variation range along with different wafer non-uniformity patterns likely inherited from the halogenation plasma (Figure 4b). The current attempts to adapt the OCD model to account for the appearance of the nucleation defects on the surface of a-C:H did not result in any consistent results. Therefore, further work involving machine learning algorithms would be needed to establish the link between the ASD process defectivity and the acquired OCD spectrum¹².

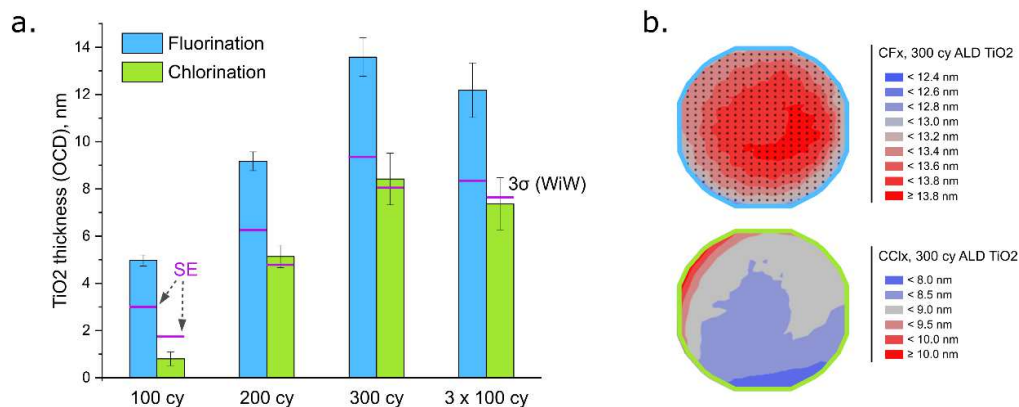


Figure 4. OCD analysis of the ASD TiO₂ process on the growth area (SiN_x) at the 90 nm pitch a-C:H line pattern: (a) OCD TiO₂ thickness in comparison with the results of spectroscopic ellipsometry (SE) measurements performed at SiN_x pattern-free areas of the same wafer; (b) OCD TiO₂ thickness wafer map.

The detection of TiO₂ on both growth and non-growth surfaces is possible by employing XPS measurement. The recorded photoelectron spectrum contains information about the chemical elements constituting the exposed surfaces with a depth down to approx. 10 nm. Moreover, XPS allows to discriminate between the TiO₂ deposited on compositionally distinct surfaces by applying an overlayer thickness quantification protocol based on attenuation of substrate-originating photoelectrons¹³. Therefore, one can in principle determine the thickness of TiO₂ deposited on top of SiN_x or halogenated a-C:H surface if there is a corresponding surface specific peak in the recorded photoelectron spectrum. The detailed scans of characteristic photoelectron peaks measured on the as-prepared a-C:H line pattern and on the patterns subjected to the halogenation plasmas are shown in Figure 5. To quantify the growth of TiO₂ on the SiN_x trench bottom, chlorinated a-C:H and fluorinated a-C:H line patterns, we observed the evolution of Si 2p, Cl 2p and F 1s peaks, respectively.

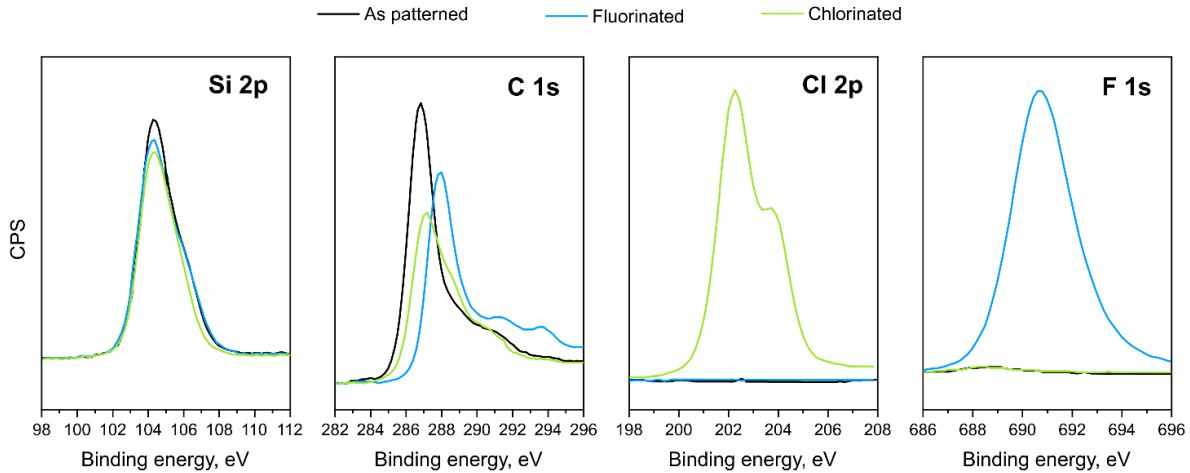


Figure 5. High-resolution XPS scans for representative element peaks recorded on 90 nm pitch a-C:H line pattern before and after the plasma halogenation.

At first, we assessed the thickness of TiO₂ deposited on top of SiN_x based on the attenuation of Si 2p peaks (Figure 6). The calculated thickness and its variation show values closely comparable to those measured by OCD on the same wafers.

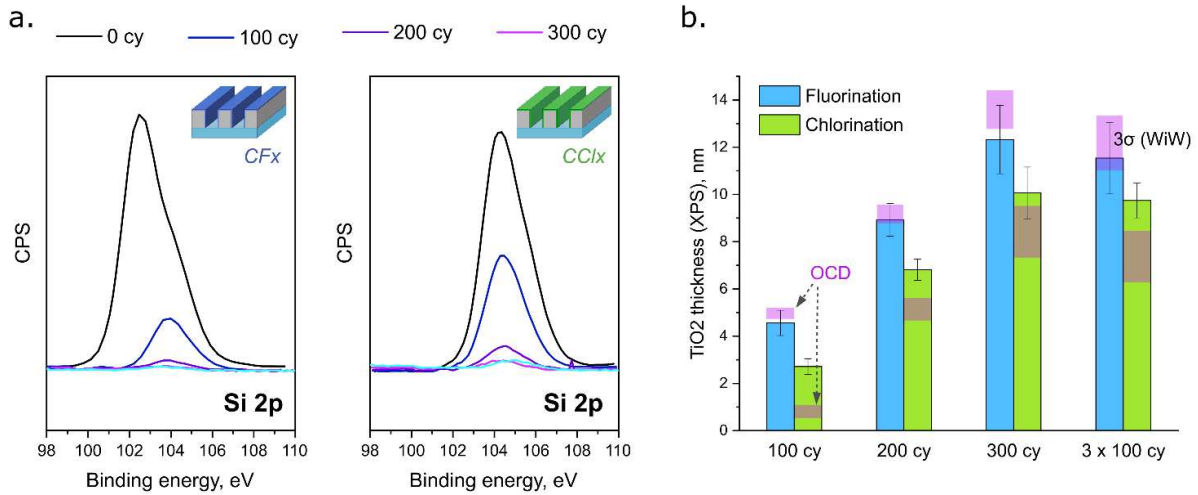


Figure 6. XPS analysis of the ASD TiO₂ process on the growth area (SiN_x) in the 90 nm pitch a-C:H line pattern: (a) evolution of Si 2p peak induced by deposition of ALD TiO₂; (b) TiO₂ thickness estimated via attenuation of Si 2p peak intensity and corresponding OCD TiO₂ thickness.

Analogously, the presence of TiO₂ on the non-growth surface was checked – the reduction of F 1s and Cl 2p peak intensity was used to estimate the thickness of the deposited TiO₂ (Figure 7a). Although in this case the accuracy of the quantitative analysis is challenged by the complex morphology of the deposited TiO₂ phase, the observed trends are in good agreement with the top-down SEM observations (Figure 7b). Interestingly, the XPS analysis shows the presence of TiO₂ on the halogenated a-C:H lines while there are no traces of TiO₂ discernable in the corresponding SEM images. While it may be attributed to higher sensitivity of XPS analysis to the TiO₂ defects, one should also consider a potential source of error in the employed defect quantification approach such as possible presence of chlorine or fluorine within the growth area in the form of functional groups attached to SiN_x surface after the halogenation plasma. More detailed study would be needed to clarify the sensitivity limits of the XPS analysis in the context of ASD processes.

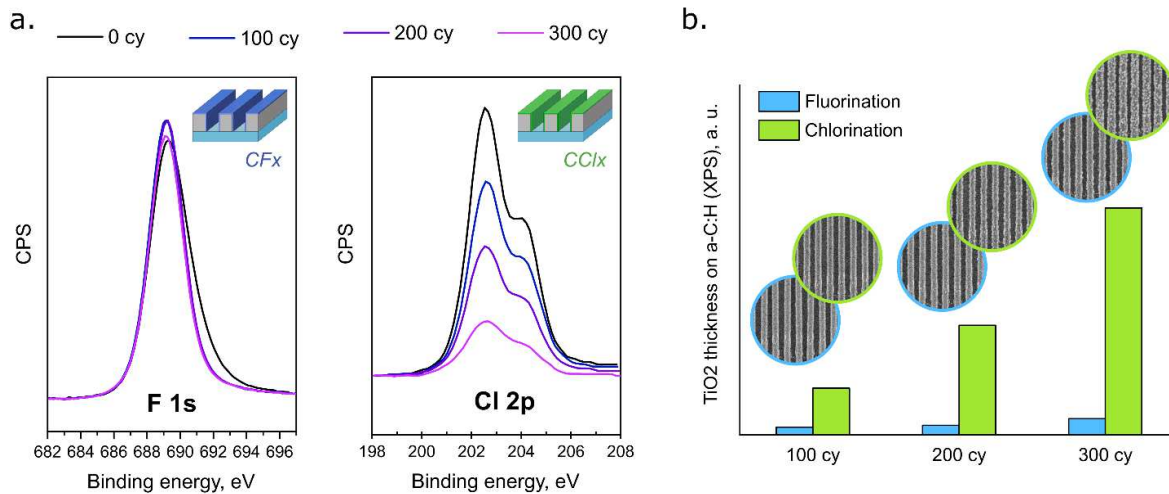


Figure 7. XPS analysis of the ASD TiO₂ process on the non-growth area (halogenated a-C:H) in the 90 nm pitch a-C:H line pattern: (a) changes in F 1s and Cl 2p signals induced by deposition of ALD TiO₂ on the surface of fluorinated and chlorinated a-C:H lines, respectively; (b) TiO₂ thickness estimated via attenuation of F 1s and Cl 2p signals.

Finally, we used the XPS analysis to investigate the origin of the significantly degraded growth inhibition potential of the a-C:H surface chlorination process on patterns. One of the plausible reasons was the presence of PEALD SiO₂ hard-mask residues on top of the a-C:H pattern, which were not removed neither by the dilute HF or by the successive chlorination plasma. As shown in p. 3.1, the fluorination with CF₄ plasma is capable of TiO₂ etching. So, we intended to test the possibility of the CF₄-plasma to remove these Si-based residues. However, to be able to check this with XPS, the interference with the Si signal from the underlying SiN_x needed to be excluded. This was achieved by applying the residue etching 60 s CF₄-plasma to the wafers which have already been processed with 300 cycles ALD TiO₂, i. e. the SiN_x layer was protected from the plasma by a thick TiO₂ film. In this test configuration, the reduction in Si 2p peak intensity could only be attributed to the removal of a Si-based material from the surface region of a-C:H lines. According to Figure 8a, the slight drop in Si 2p peak intensity was detected only on the chlorinated a-C:H pattern, which favors the hypothesis about the adverse role of the hard-mask residues and at the same time suggests a potential solution for enhancement of the process selectivity. The optimized chlorination process of a-C:H line pattern including an additional CF₄-plasma pre-cleaning step demonstrated significantly reduced density of TiO₂ nucleation defects on the a-C:H surface (Figure 8b).

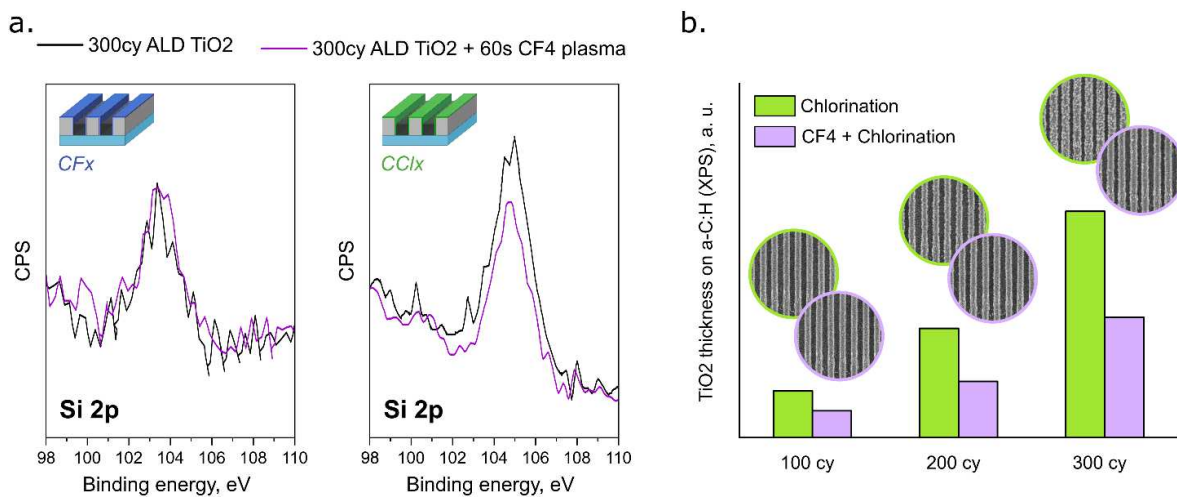


Figure 8. Adverse effect of hard-mask residues on selectivity of ALD TiO₂ process featuring chlorinated a-C:H line pattern: (a) Si 2p XPS signals recorded after deposition of 300 cycles ALD TiO₂ and after additional exposure to CF₄ plasma; (b) the effect of CF₄ plasma pre-treatment on the TiO₂ defects formed over the non-growth area (chlorinated a-C:H) assessed by XPS and top-down SEM.

4. CONCLUSIONS

To summarize, we demonstrated that the plasma halogenated amorphous carbon can be employed as an efficient growth inhibition layer in ASD processes. In turn, the blocking efficiency of the plasma halogenation on patterns was shown to strongly depend on its ability to regenerate the a-C:H surface. In this aspect, the fluorination process outperforms the chlorination treatment which exhibits superior selectivity on blanket a-C:H films. The use of OCD and XPS in-line metrology techniques throughout the study highlights their complementary nature and comprehensiveness for evaluation, monitoring and optimization of an ASD process. The XPS analysis provides quantitative information about the deposition on both growth and non-growth surfaces, while OCD enables quick thickness mapping of the selectively deposited film in the growth area. The limits of these in-line metrology techniques in the context of their sensitivity to the ASD process defects is a subject of future research.

ACKNOWLEDGEMENT

This project has received funding from the ECSEL Joint Undertaking (JU) under grant agreement No 783247. The JU receives support from the European Union's Horizon 2020 research and innovation program in Netherlands, Belgium, Germany, France, Italy, Austria, Hungary, Romania, Sweden and Israel.

REFERENCES

- [1] Minaye Hashemi, F. S., Birchansky, B. R. and Bent, S. F., "Selective Deposition of Dielectrics: Limits and Advantages of Alkanethiol Blocking Agents on Metal–Dielectric Patterns," *ACS Appl. Mater. Interfaces* **8**(48), 33264–33272 (2016).
- [2] Liu, T.-L. and Bent, S. F., "Area-selective atomic layer deposition of dielectric-on-dielectric for Cu/low-k dielectric patterns," *Adv. Patterning Mater. Process.* XXXVI(May 2019), R. Gronheid and D. P. Sanders, Eds., 23, SPIE (2019).
- [3] Stevens, E., Tomczak, Y., Chan, B. T., Altamirano Sanchez, E., Parsons, G. N. and Delabie, A., "Area-Selective Atomic Layer Deposition of TiN, TiO₂, and HfO₂ on Silicon Nitride with inhibition on Amorphous Carbon," *Chem. Mater.* **30**(10), 3223–3232 (2018).
- [4] Simon, A. H., Bolom, T., Niu, C., Baumann, F. H., Hu, C., Parks, C., Nag, J., Kim, H., Lee, J. Y., Yang, C., Nguyen, S., Shobha, H. K., Nogami, T., Guggilla, S., Ren, J., Sabens, D. and AuBuchon, J. F., "Electromigration comparison of selective CVD cobalt capping with PVD Ta(N) and CVD cobalt liners on 22nm-groundrule dual-damascene Cu interconnects," 2013 IEEE Int. Reliab. Phys. Symp.(c), 3F.4.1-3F.4.6, IEEE (2013).
- [5] Hong, J., Porter, D. W., Sreenivasan, R., McIntyre, P. C. and Bent, S. F., "ALD Resist Formed by Vapor-Deposited Self-Assembled Monolayers," *Langmuir* **23**(3), 1160–1165 (2007).
- [6] Schreiber, F., "Structure and growth of self-assembling monolayers," *Prog. Surf. Sci.* **65**, 151–256 (2000).
- [7] Vallat, R., Gassilloud, R., Eychenne, B. and Vallée, C., "Selective deposition of Ta₂O₅ by adding plasma etching super-cycles in plasma enhanced atomic layer deposition steps," *J. Vac. Sci. Technol. A Vacuum, Surfaces, Film.* **35**(1), 01B104 (2017).
- [8] Vos, M. F. J., Chopra, S. N., Verheijen, M. A., Ekerdt, J. G., Agarwal, S., Kessels, W. M. M. and Mackus, A. J. M., "Area-Selective Deposition of Ruthenium by Combining Atomic Layer Deposition and Selective Etching," *Chem. Mater.* **31**(11), 3878–3882 (2019).
- [9] Parsons, G. N., "Functional model for analysis of ALD nucleation and quantification of area-selective deposition," *J. Vac. Sci. Technol. A* **37**(2), 020911 (2019).
- [10] Spampinato, V., Armini, S., Franquet, A., Conard, T., van der Heide, P. and Vandervorst, W., "Self-focusing SIMS: A metrology solution to area selective deposition," *Appl. Surf. Sci.* **476**(January), 594–599 (2019).
- [11] Nečas, D. and Klapetek, P., "Gwyddion: an open-source software for SPM data analysis," *Open Phys.* **10**(1), 181–188 (2012).
- [12] Timoney, P. R., Kagalwala, T., Reis, E., Lazkani, H., Hurley, J., Kang, C., Isbester, P., Liu, H., Yellai, N., Shifrin, M. and Etzioni, Y., "Implementation of machine learning for high-volume manufacturing metrology challenges (Conference Presentation)," *Metrol. Insp. Process Control Microlithogr.* XXXII **m**(May), O. Adan and V. A. Ukraintsev, Eds., 32, SPIE (2018).
- [13] Powell, C. J. and Jablonski, A., "Progress in quantitative surface analysis by X-ray photoelectron spectroscopy: Current status and perspectives," *J. Electron Spectros. Relat. Phenomena* **178–179**(C), 331–346 (2010).